



HHS Public Access

Author manuscript

Neuroimage. Author manuscript; available in PMC 2017 August 08.

Published in final edited form as:

Neuroimage. 2017 August 01; 156: 146–154. doi:10.1016/j.neuroimage.2017.05.025.

Transcranial manganese delivery for neuronal tract tracing using MEMRI

Tatjana Atanasijevic^{a,*}, Nadia Bouraoud^a, Dorian B. McGavern^b, and Alan P. Koretsky^a

^aLaboratory of Functional and Molecular Imaging, National Institute of Neurological Disorders and Stroke, National Institutes of Health, Bethesda, MD 20892, USA

^bLaboratory of Viral Immunology and Intravital Imaging, National Institute of Neurological Disorders and Stroke, National Institutes of Health, Bethesda, MD 20892, USA

Abstract

There has been a growing interest in the use of manganese-enhanced MRI (MEMRI) for neuronal tract tracing in mammals, especially in rodents. For this MEMRI application, manganese solutions are usually directly injected into specific brain regions. Recently it was reported that manganese ions can diffuse through intact rat skull. Here the local manganese concentrations in the brain tissue after transcranial manganese application were quantified and the effectiveness of tracing from the area under the skull where delivery occurred was determined. It was established that transcranially applied manganese yields brain tissue enhancement dependent on the location of application on the skull and that manganese that enters the brain transcranially can trace to deeper brain areas.

Keywords

MEMRI; tract tracing; transcranial delivery

Introduction

Manganese is an essential element that has fundamental roles in cellular processes in living organisms, especially in brain function (Aschner et al., 2006). Mn^{2+} has similar ionic radius as Ca^{2+} and behaves as a Ca^{2+} analog (Merritt et al., 1989; Narita et al., 1990). Thus, Mn^{2+} can enter excitable cells such as neurons via L-type voltage-gated Ca^{2+} channels (Narita et al., 1990; Pautler, 2006) and can activate N-methyl-D-aspartate glutamate receptors (Gobbo et al., 2012). Once inside neurons, Mn^{2+} is transported along the axons in a microtubule dependent manner and gets released into the synaptic cleft, where it gets taken up by the next neuron in the neural circuit (Sloot and Gramsbergen, 1994; Pautler et al., 1998, 2003; Takeda et al., 1998; Pautler and Koretsky, 2002). Moreover, Mn^{2+} is a paramagnetic ion and acts as an excellent contrast agent in magnetic resonance imaging (MRI) (Mendonca-Dias et al., 1983; Geraldès et al., 1986; Cory et al., 1987). Accumulation of Mn^{2+} in a tissue leads to shortening of the spin-lattice relaxation time, T_1 , and the spin-spin relaxation time, T_2 , of

*Correspondence to: National Institute of Neurological Disorders and Stroke, National Institutes of Health, 10 Center Drive, Bldg. 10, Rm. 1D48, MD 20892, USA.

water molecules in that tissue. T_1 relaxivity is typically more sensitive than T_2 relaxivity for MRI at higher magnetic fields. Shortening of T_1 of the tissue in which Mn^{2+} accumulates results in a positive contrast enhancement in T_1 -weighted MRI of that tissue. These combined properties of Mn^{2+} have led to use of manganese-enhanced MRI (MEMRI) in the past couple of decades in a large variety of studies. Presently, there are three major uses of MEMRI in the brain: for enhancement of brain cytoarchitecture in anatomical studies (Natt et al., 2002; Watanabe et al., 2002, 2004; Aoki et al., 2004b), for mapping neuronal activity (Lin and Koretsky, 1997; Aoki et al., 2002, 2004a; Hsu et al., 2007; Yu et al., 2008) and for *in vivo* tracing of neuronal connections (Pautler et al., 1998, 2003; Van der Linden et al., 2002). The use of MEMRI for anatomy and function extends to other tissues as well, such as heart (Hu et al., 2001), pancreas (Gimi et al., 2006) and tumors (Banerjee et al., 2007; Hasegawa et al., 2011).

The first study to use MEMRI for neuronal tract tracing focused on tracing of olfactory and visual pathways in mouse brain (Pautler et al., 1998). Since then, many MEMRI tract tracing studies have been successfully performed on different neural pathways and species, such as the song control pathway in songbirds (Van der Linden et al., 2002, 2004), olfactory pathway in rats (Cross et al., 2004; Chuang and Koretsky, 2006), visual pathway in rats and nonhuman primates (Watanabe et al., 2001; Thuen et al., 2005; Murayama et al., 2006), somatosensory pathway in rats (Allegrini and Wiessner, 2003; Leergaard et al., 2003), basal ganglia pathway in macaques, mice and rats (Saleem et al., 2002; Pautler et al., 2003; Pelled et al., 2007), auditory pathway in guinea pigs (Lee et al., 2007) and corticospinal pathway in rats and marmosets (Bilgen et al., 2006; Demain et al., 2015). For neuronal tract tracing, Mn^{2+} solutions are usually directly injected into specific brain or peripheral areas, or delivered nasally when tracing olfactory pathways.

A recent study of traumatic brain injury (TBI) has shown that small molecular weight fluorescent molecules as well as dextrans of various sizes can diffuse through intact murine skull into the meningeal space (Roth et al., 2014). Meningeal concentrations of these molecules were found to be dependent on the size of the applied molecules and length of the application to the thinned skull. This method of substance delivery to the brain is called transcranial application. In addition to fluorescent probes, several purinergic receptors and manganese solutions were demonstrated to reach the brain with transcranial application. In the case of $MnCl_2$, MRI enhancement was detected below the area of the brain where the $MnCl_2$ was applied. In that study, the Mn^{2+} passage through the intact rat skull was demonstrated but not well characterized. The purpose of this study was to determine the factors that affect transcranially applied Mn^{2+} and determine whether the Mn^{2+} that enters the brain can be used to trace neural systems.

Materials and methods

Animal preparation

Adult male Sprague-Dawley rats (body weights 200–300 g), obtained from Harlan Laboratories, were used for this study. The animals were provided Open Formula Rat and Mouse Diet (NIH-07). All animal work was performed according to the guidelines of the Animal Care and Use Committee of National Institute of Neurological Disorders and Stroke,

National Institutes of Health (Bethesda, MD). The rats were initially anesthetized with 5% isoflurane, and then switched to 1–2% isoflurane for maintenance throughout the procedure. Body temperature was monitored and maintained by a heated water bath. As previously described (Roth et al., 2014), animals were placed in a stereotaxic apparatus and a single midline incision with a sterile scalpel was made through the skin above the skull. The skull bone was exposed by scraping away the periosteum and bleeding was stopped with a surgical cauterizer. Sterile saline (0.9% NaCl) solutions of MnCl₂ (Sigma-Aldrich, St. Louis, MO), of concentrations ranging from 0 to 500 mM, were placed directly on the skull bone, in various locations, to investigate the efficiency of manganese passage through the different regions of the skull. Specific targeted areas are illustrated in the first figure. Pure saline was used as a control. Solutions of CaCl₂, NaCl, MgCl₂ and D-mannitol (Sigma-Aldrich, St. Louis, MO) in different concentrations were each separately added to some of the MnCl₂ solutions to study the possible effect of ionic strength and osmolarity on the delivery efficiency. The solutions were pipetted on the rat skull over a 2-h period in 5- μ l aliquots and replenished as needed. The total volume of applied MnCl₂ solutions did not exceed 50 μ l. After 2 h the skin was sutured and the animal promptly placed in a MRI scanner to detect manganese diffusion into the brain. In some cases, MRI was also performed one day later to determine if there was tracing of the Mn²⁺ along appropriate neural pathways. A group of three rats was used for each set of experimental conditions.

MRI data acquisition

Images were acquired on an 11.7 T/31 cm horizontal magnet (Agilent, Oxford, UK) interfaced to a Bruker Avance III console (Bruker BioSpin, Billerica, MA) equipped with a 12-cm gradient set (Resonance Research Inc., Billerica, MA). A 9-cm laboratory-built birdcage coil was used for signal transmission and a 2-cm surface coil placed on the rat head was used for signal reception. During imaging, anesthesia was maintained at 1.5% isoflurane and the animal body temperature was maintained at 37 °C via a temperature-controlled heated water bath. Animals were imaged immediately after manganese administration, as well as 24 h later for tracing experiments. Thirty, 1-mm-thick, axial MRI slices were acquired across the brain. A T₁-weighted spin echo pulse sequence (TE=7.6 ms, TR=500 ms, Nav=8, 100 μ m in-plane resolution, 19 min total scan duration) was used to detect contrast enhancement by manganese. The T₁ relaxation times were measured using a saturation recovery spin-echo sequence (TE=7.6 ms, TRs=0.4; 0.97; 1.77; 3.124 and 10 s, Nav=2, 200 μ m in-plane resolution, 78 min total scan duration).

MRI image analysis

MRI data obtained from rats receiving transcranial manganese were analyzed using ImageJ (<http://rsb.info.nih.gov/ij/>) and MIPAV (<http://mipav.cit.nih.gov/>) software developed at NIH. T₁ relaxation maps for brain slices were calculated using the MRI Analysis Calculator plugin in ImageJ software. Background tissue T₁ values and standard deviations for every slice were obtained by placing a region of interest (ROI) over an area of the cortex away from the one of manganese administration. T₁ relaxation maps were thresholded using the value of the background T₁ minus two standard deviations to obtain ROIs in which manganese had significantly shortened the T₁ of the cortex tissue for the calculations in Figs. 3 and 4. Total amounts of manganese in the whole volume have been calculated by

adding all the amounts in the relevant slices. For quantification of manganese tracing in Fig. 6, ROIs were obtained by overlapping MR images obtained using saturation recovery spin-echo sequence with registered rat brain atlas (adapted from Paxinos and Watson (2007), 6th edition) similarly as previously described (Yu et al., 2012; Yu and Koretsky, 2014). The same thalamus ROIs were used for all experiments investigating the same neuronal tract, thus two different thalamus ROIs were determined for the two different pathways studied in these experiments, somato-motor and visual. A single ROI was used for quantification of hippocampal signal. These ROIs were then placed on the calculated T_1 relaxation maps for quantification. The average T_1 relaxation times as well as the total number of voxels in all the ROIs were used to determine the local concentration and total amount of manganese in each slice, using the equation: $1/(T_1)_{\text{observed}} = 1/(T_1)_{\text{background}} + r_1 \times c$, where c is the concentration of the contrast agent (typically expressed in mM) and r_1 is its relaxivity: an intrinsic ability of a contrast agent to change the longitudinal relaxation rate of a certain tissue (typically expressed in $s^{-1} \text{ mM}^{-1}$). The value of $4.7 \text{ s}^{-1} \text{ mM}^{-1}$ was used for cortical T_1 relaxivity as previously reported (Chuang et al., 2009). All the calculated data points are averages of the calculations from three ROIs, each ROI uniquely corresponding to one of the three animals in the group for a particular set of experimental conditions. All the data are represented as mean \pm standard deviation. Statistical t -tests were performed to investigate the significance of transcranial delivery effects: unpaired two-tailed t -test was used to compare the group of rats receiving 100 mM MnCl_2 on the bregma vs. rats receiving 100 mM $\text{MnCl}_2 + 400 \text{ mM CaCl}_2$ on the bregma; while the paired one-tailed t -test was used to compare values of T_1 in the thalamus ROIs between immediately after the manganese application and 24 h later for all the tracing experiments. One tailed paired t -test was used in the latter case since contrast agents are expected to only decrease relaxation times.

Results

Recently, it was reported that manganese ions can diffuse through intact rat skull (Roth et al., 2014). Here, the local manganese amounts in the brain tissue after transcranial manganese application were quantified and the effectiveness of tracing from different skull areas was determined.

The effectiveness of the manganese diffusion through different regions of intact rat skull is demonstrated by the images in Fig. 1, where hyperintense regions represent cortical areas with significant manganese concentrations. Manganese can diffuse readily to levels that produce detectable tissue enhancement by MRI through areas of the skull that contain or are near suture lines where the adjacent skull bone plates come together, such as bregma (Fig. 1B) and lambda (Fig. 1C). Conversely, very limited manganese passage through the skull is detected when manganese is applied to skull areas away from the sutures (Fig. 1D and E).

When applied on bregma, the total amount of manganese in a MRI slice with most efficient delivery is proportional to the manganese concentration applied (Fig. 2). No detectable cortex manganese was observed for 100 mM applied manganese solution. To investigate a possible roll for total osmolarity in the manganese delivery, CaCl_2 was added to various concentrations of MnCl_2 in such a manner that the total salt concentration equaled 500 mM (Fig. 3E). The addition of calcium had a significant effect because applied manganese

concentrations that were previously undetectable in the cortex, such as 100 mM (Fig. 3A and B), became detectable ($p=0.009$ for comparison of rats receiving 100 mM manganese solution with or without calcium addition). Moreover, concentrations as low as 10 mM manganese became observable with MRI.

To examine if this enhancing effect is unique to calcium, other secondary salts as well as mannitol were added to 100 mM solution of $MnCl_2$ (Fig. 4A). Substituting $CaCl_2$ solution with $NaCl$ solution of equal ionic strength or $MgCl_2$ solution of the same concentration led to much less efficient delivery of manganese. Addition of mannitol, a substance commonly used to increase the osmolarity of a solution and often used to transiently open the blood brain barrier, to the $MnCl_2$ solution did not significantly aid the transcranial manganese delivery. Therefore, it appears that augmentation of the efficiency of manganese delivery through the skull is specific to calcium. To further investigate this effect, the amount of added calcium to a solution of low manganese concentration was lowered, and the efficiency of manganese delivery at concentrations lower than 300 mM quickly diminished with lower calcium concentrations (Fig. 4B).

To determine if manganese delivered through the skull would trace neural connections similar to when $MnCl_2$ is directly injected into the rodent brain, motor/somatosensory and visual cortex were loaded through the skull. Manganese was applied proximate to bregma to target the motor/somatosensory cortex and proximate to lambda to target the visual cortex. Significant shortenings of T_1 in the motor/somatosensory ($p=0.03$, 0.001 and 0.02, respectively, for rats receiving for 500 mM $MnCl_2$, 250 mM $MnCl_2$, and 100 mM $MnCl_2+400$ mM $CaCl_2$ on the bregma) and visual thalamus areas ($p=0.045$ for rats receiving 250 mM $MnCl_2+250$ mM $CaCl_2$ on the lambda) were observed 24 h later (Figs. 5 and 6). This is consistent with previous work where enhancement of MRI signal in the thalamus was observed 10 h after focal injection of manganese in the rat somatosensory cortex (Leergaard et al., 2003), as well as 24 h after manganese was injected in the rat eye (Watanabe et al., 2001). The total amount of manganese in the thalamus and hippocampus ROIs was quantified for both neuronal pathways (Fig. 6). Measurements in the hippocampus ROI were used as a control for systemic delivery of manganese, since hippocampus signal enhances through systemic delivery of manganese through cerebrospinal fluid (CSF) and possibly blood. A signal enhancement in the pituitary gland, indicative of systemic manganese delivery through the blood, was observed both in the MR images taken right after the application as well as 24 h later (images not shown). In the present work, of all the manganese that reached the cortex following application of a 500 mM solution of $MnCl_2$ to bregma, approximately 6% ended up in the thalamus ROI and 1.3% in the hippocampus ROI the following day. This suggests that the major part of thalamus signal enhancement was due to tract tracing of manganese from the cortex, and minor part due to the systemic delivery through the vasculature and CSF. When manganese solution was applied on the lambda, the amounts in hippocampus and thalamus appear close but direct comparison with bregma application is not possible as different experimental conditions (type and concentration of applied solutions) were used. If it is desired to account for the non-specific signal enhancement in the tract tracing experiments, normalization by the pituitary signal can be employed as previously reported (Chuang and Koretsky, 2009). Tract tracing is most efficient at highest manganese concentrations applied to the skull, but lower manganese

concentrations can be successfully used for tracing if appropriate calcium amounts are added.

Discussion

The findings demonstrate that manganese ions can pass through intact rat skull and thus be delivered to the brain by simple application on the skull. This is a much less invasive method of manganese delivery to the brain than traditional methods such as intracerebral injection. Once in the brain tissue, this contrast agent behaves in a similar manner as when introduced via the common invasive delivery methods and can therefore be used for neuronal tract tracing.

Manganese ions can pass most efficiently through areas of the skull that contain suture lines such as bregma, whereas normal skull bone is much less permeable to manganese ions under conditions used in this study. Because these fissure lines may contain space where the bones come together and are typically rich with blood vessels, diffusion around the blood vessels in these regions may be a possible contributor to the mechanism of the manganese passage through intact rat skull. Once through the skull, manganese penetrates the meninges to enter cortical tissue. The mechanism whereby manganese penetrates the meninges is not clear and it could be passing through the vessels that enter and exit meninges or via transcellular pathways. Indeed, it is well known that liver will uptake Mn^{2+} and transport it into bile and choroid plexus will uptake manganese and transport it into CSF via transcellular pathways.

Concentrated solutions of $MnCl_2$, such as 500 mM and 250 mM used in this study, are of high osmolarity and can pass through the intact rat skull. Solutions of lower manganese concentration were able to successfully diffuse through the skull bone only upon the addition of calcium salts. This suggests that the rate limiting step of the transcranial manganese delivery is passage through the skull and the meninges. This effect could not be mimicked either by addition of salts of other divalent (magnesium) and monovalent (sodium) cations or by addition of chemicals that increase osmolarity (mannitol). These findings, in conjunction with the observation that the total amount of delivered manganese saturates when the applied salt concentrations are high, suggest that this delivery process is saturable and likely not due to passive diffusion alone. Of the substances we tried, only calcium can enhance the efficiency of manganese delivery through the intact rat skull into the brain, though it is unclear how exactly calcium aids manganese in its passage through the skull and into the brain. It could be that divalent Ca^{2+} saturates Mn^{2+} binding sites in bones which are of high phosphate content, or causes cell volume changes or disrupts cellular structure in either the bone or meninges.

The skull area covered by the pipetted drops of manganese solution was typically of an elliptical shape, with approximately a 3 mm major axis and a 2 mm minor axis. It was not possible to control the drop spread very rigorously and thus there is variability between animals in the same group represented by larger standard deviations. While a small number of animals were used in each group (three), the effects were large which makes statistical comparison between different treatments still possible. A comparison between rats receiving 100 mM $MnCl_2$ on the bregma vs. rats receiving 100 mM $MnCl_2$ +400 mM $CaCl_2$ on the

bregma showed that the difference in amount of delivered manganese is significant ($p=0.009$), confirming that addition of calcium significantly improves efficiency of transcranial manganese delivery. There was a group of three animals receiving 50 mM $MnCl_2+100$ mM $CaCl_2$ (Fig. 4B) where no animals had voxels above the threshold. In general, the number of voxels above the threshold for animals receiving low concentrations of manganese was fairly small and relatively difficult to precisely determine due to the surgical artifacts on the top of the skull. Nevertheless, this error is fairly small, as control animals that had no manganese but display surgical artifacts had no voxels above the threshold, indicating surgical artifacts were not a large error.

It is worthwhile noting that in the MRI slices with the most efficient manganese delivery, darkening was observed in the areas of the brain right under the skull when higher concentrations of manganese (500 mM) were applied. This was likely due to T_2 shortening effects from high local manganese concentrations. This effect was not observed when lower manganese concentrations (100 mM) were applied directly through the skull. Some relevant voxels may have been omitted in the data analysis due to this artifact. However, the number of such voxels is very low compared to the total volume and a much smaller source of error than variability of delivery efficiency under the same experimental conditions. If the effects of high concentration of Mn^{2+} at the delivery site are of concern in quantitative tracing experiments, then lower manganese concentrations can be used for the tracing experiments with the addition of the appropriate amounts of calcium to enhance the delivery efficiency. Generally, it was noted that there is a large distribution of T_1 values in the ROIs in the brain, which was correlated to the distance from the skull area where manganese was applied. Therefore, more sophisticated calculation methods to determine local manganese concentrations than the average T_1 in the ROI used here may be needed in tracing studies where very precise quantification is required.

Manganese can act as a neurotoxin at high enough concentrations (Aschner and Aschner, 1991). It has been demonstrated that injections of high manganese concentrations (800 mM) directly into to the cortex of a monkey can lead to neuronal loss in the areas directly adjacent to the injection site, whereas injection of lower manganese concentrations (120 mM) into the cortex allowed for neuronal tract tracing with little or no toxicity or adverse changes in animal behavior (Simmons et al., 2008). Still, no adverse gross behavioral changes were observed in our rat studies even with the highest transcranially applied manganese concentration of 500 mM. The animals were monitored for up to three weeks after the contrast agent application. This is consistent with our estimation that less than 0.01% of transcranially applied manganese reaches the brain, and that the average local concentrations of manganese in the ROIs in the brain rarely exceed 200 μM for the highest transcranially applied manganese concentration of 500 mM. Cellular studies indicate toxicity begins above the 200 μM manganese concentration in neural tissue (Daoust et al., 2015).

Transcranial manganese delivery can be used as an alternative, much less invasive method to deliver manganese to the brain for neuronal tract tracing studies. Presently, this is limited to only certain areas of the brain, and the precision of the application is not very good. Since manganese is most efficiently delivered through the sutures, cortical areas directly underlying the sutures or very proximate to them are the most amenable to tract tracing

studies using transcranial manganese delivery. These areas include motor, somatosensory and visual cortex, which were transcranially loaded in the current study, as well as other cortical areas, such as cingulate and retrosplenial dysgranulate cortex. Our method of placing manganese on the skull is relatively crude as it involves pipetting a small drop of the solution on a desired location on the skull, the spread of which cannot be controlled well. We are currently working on designing bottomless cups of small radii that could temporarily be fixed on a desired spot on a rat skull so that the manganese solution can be contained on the precise location on the skull by the cup throughout the delivery and its interaction with nearby skin minimized. This would constitute a more controlled approach to the delivery than simple direct pipetting. Thus, the precision of application and access to any skull area may be improved by building more sophisticated delivery cups as opposed to simply placing Mn^{2+} onto the exposed skull. Indeed, in some of the experiments in the original description of the transcranial delivery of dextrans and fluorescent compounds, the mouse skull was thinned (Roth et al., 2014) and thus thinning of the rat skull could also significantly increase the efficiency of transcranial delivery. In that study, fluorescent dextrans of MW up to 40,000 were successfully detected in mouse meninges. Thus, we are currently investigating the possibility of transcranial delivery through the rat skull of substances with larger MW than Mn^{2+} ion, such as Gd chelates as well as some drugs that do not generate MR contrast. The transcranial delivery method may also be very useful in tracing studies where adverse effects from direct manganese injection interfere with the process investigated. Other compounds, such as various drugs for treatment of brain cancer or neurodegenerative diseases, may be possible to deliver to the brain in this manner as well.

In conclusion, intact rat skull is permeable to manganese ions. This may open a whole new and less invasive path for brain delivery of various contrast agents and drugs as well as provide much less invasive manganese delivery method for MEMRI-based tract tracing in the brain.

Acknowledgments

This research was supported by the Intramural Research Program of the NIH, NINDS. The authors would like to thank Dr. Doug Morris for help with CT imaging, as well as Dr. Steve Dodd for providing MRI technical support.

References

- Allegrini PR, Wiessner C. Three-dimensional MRI of cerebral projections in rat brain in vivo after intracortical injection of $MnCl_2$. *NMR Biomed.* 2003; 16:252–256. <http://dx.doi.org/10.1002/nbm.834>. [PubMed: 14648884]
- Aoki I, Naruse S, Tanaka C. Manganese-enhanced magnetic resonance imaging (MEMRI) of brain activity and applications to early detection of brain ischemia. *NMR Biomed.* 2004a; 17:569–580. <http://dx.doi.org/10.1002/nbm.941>. [PubMed: 15617055]
- Aoki I, Tanaka C, Takegami T, Ebisu T, Umeda M, Fukunaga M, Fukuda K, Silva AC, Koretsky AP, Naruse S. Dynamic activity-induced manganese-dependent contrast magnetic resonance imaging (DAIM MRI). *Magn. Reson. Med.* 2002; 48:927–933. <http://dx.doi.org/10.1002/mrm.10320>. [PubMed: 12465100]
- Aoki I, Wu YJ, Silva AC, Lynch RM, Koretsky AP. In vivo detection of neuroarchitecture in the rodent brain using manganese-enhanced MRI. *NeuroImage.* 2004b; 22:1046–1059. <http://dx.doi.org/10.1016/j.neuroimage.2004.03.031>. [PubMed: 15219577]

- Aschner M, Aschner JL. Manganese neurotoxicity: cellular effects and blood-brain barrier transport. *Neurosci. Biobehav. Rev.* 1991; 15:333–340. [PubMed: 1956602]
- Aschner M, Lukey B, Tremblay A. The Manganese Health Research Program (MHRP): status report and future research needs and directions. *Neurotoxicology.* 2006; 27:733–736. <http://dx.doi.org/10.1016/j.neuro.2005.10.005>. [PubMed: 16325914]
- Banerjee D, Hegedus B, Gutmann DH, Garbow JR. Detection and measurement of neurofibromatosis-1 mouse optic glioma in vivo. *NeuroImage.* 2007; 35:1434–1437. <http://dx.doi.org/10.1016/j.neuroimage.2007.02.019>. [PubMed: 17383899]
- Bilgen M, Peng W, Al-Hafez B, Dancause N, He YY, Cheney PD. Electrical stimulation of cortex improves corticospinal tract tracing in rat spinal cord using manganese-enhanced MRI. *J. Neurosci. Methods.* 2006; 156:17–22. <http://dx.doi.org/10.1016/j.jneumeth.2006.02.001>. [PubMed: 16530270]
- Chuang KH, Koretsky A. Improved neuronal tract tracing using manganese enhanced magnetic resonance imaging with fast T(1) mapping. *Magn. Reson. Med.* 2006; 55:604–611. <http://dx.doi.org/10.1002/mrm.20797>. [PubMed: 16470592]
- Chuang KH, Koretsky AP. Accounting for nonspecific enhancement in neuronal tract tracing using manganese enhanced magnetic resonance imaging. *Magn. Reson. Imaging.* 2009; 27:594–600. <http://dx.doi.org/10.1016/j.mri.2008.10.006>. [PubMed: 19144489]
- Chuang KH, Koretsky AP, Sotak CH. Temporal changes in the T1 and T2 relaxation rates (DeltaR1 and DeltaR2) in the rat brain are consistent with the tissue-clearance rates of elemental manganese. *Magn. Reson. Med.* 2009; 61:1528–1532. <http://dx.doi.org/10.1002/mrm.21962>. [PubMed: 19353652]
- Cory DA, Schwartzentruber DJ, Mock BH. Ingested manganese chloride as a contrast agent for magnetic resonance imaging. *Magn. Reson. Imaging.* 1987; 5:65–70. [PubMed: 3586874]
- Cross DJ, Minoshima S, Anzai Y, Flexman JA, Keogh BP, Kim Y, Maravilla KR. Statistical mapping of functional olfactory connections of the rat brain in vivo. *NeuroImage.* 2004; 23:1326–1335. <http://dx.doi.org/10.1016/j.neuroimage.2004.07.038>. [PubMed: 15589097]
- Daoust A, Barbier EL, Bohic S, Stupar V, Maunoir-Regimbal S, Fauvelle F. Impact of manganese on the hippocampus metabolism in the context of MEMRI: a proton HRMAS MRS study. *Toxicol. Res.-UK.* 2015; 4:376–384. <http://dx.doi.org/10.1039/c4tx00135d>.
- Demain B, Davoust C, Plas B, Bolan F, Boulanouar K, Renaud L, Darmana R, Vaysse L, Vieu C, Loubinoux I. Corticospinal tract tracing in the marmoset with a clinical whole-body 3 T scanner using manganese-enhanced MRI. *PLoS One.* 2015; 10:e0138308. <http://dx.doi.org/10.1371/journal.pone.0138308>. [PubMed: 26398500]
- Geraldes CF, Sherry AD, Brown RD 3rd, Koenig SH. Magnetic field dependence of solvent proton relaxation rates induced by Gd3+ and Mn2+ complexes of various polyaza macrocyclic ligands: implications for NMR imaging. *Magn. Reson. Med.* 1986; 3:242–250. [PubMed: 3086656]
- Gimi B, Leoni L, Oberholzer J, Braun M, Avila J, Wang Y, Desai T, Philipson LH, Magin RL, Roman BB. Functional MR microimaging of pancreatic beta-cell activation. *Cell Transplant.* 2006; 15:195–203. [PubMed: 16719054]
- Gobbo OL, Petit F, Gurden H, Dhenain M. In vivo detection of excitotoxicity by manganese-enhanced MRI: comparison with physiological stimulation. *Magn. Reson. Med.* 2012; 68:234–240. <http://dx.doi.org/10.1002/mrm.23210>. [PubMed: 22127903]
- Hasegawa S, Saito S, Koshikawa-Yano M, Furukawa T, Aoki I, Saga T. Tumor enhancement effect of overexpressed manganese-superoxide dismutase in manganese-enhanced MR imaging. *Magn. Reson. Med. Sci.* 2011; 10:155–158. [PubMed: 21959997]
- Hsu YH, Lee WT, Chang C. Multiparametric MRI evaluation of kainic acid-induced neuronal activation in rat hippocampus. *Brain.* 2007; 130:3124–3134. <http://dx.doi.org/10.1093/brain/awm207>. [PubMed: 17785345]
- Hu TC, Pautler RG, MacGowan GA, Koretsky AP. Manganese-enhanced MRI of mouse heart during changes in inotropy. *Magn. Reson. Med.* 2001; 46:884–890. [PubMed: 11675639]
- Lee JW, Park JA, Lee JJ, Bae SJ, Lee SH, Jung JC, Kim MN, Lee J, Woo S, Chang Y. Manganese-enhanced auditory tract-tracing MRI with cochlear injection. *Magn. Reson. Imaging.* 2007; 25:652–656. <http://dx.doi.org/10.1016/j.mri.2006.10.003>. [PubMed: 17540276]

- Leergaard TB, Bjaalie JG, Devor A, Wald LL, Dale AM. In vivo tracing of major rat brain pathways using manganese-enhanced magnetic resonance imaging and three-dimensional digital atlas. *NeuroImage*. 2003; 20:1591–1600. [PubMed: 14642470]
- Lin YJ, Koretsky AP. Manganese ion enhances T1-weighted MRI during brain activation: an approach to direct imaging of brain function. *Magn. Reson. Med*. 1997; 38:378–388. [PubMed: 9339438]
- Mendonca-Dias MH, Gaggelli E, Lauterbur PC. Paramagnetic contrast agents in nuclear magnetic resonance medical imaging. *Semin. Nucl. Med*. 1983; 13:364–376. [PubMed: 6359418]
- Merritt JE, Jacob R, Hallam TJ. Use of manganese to discriminate between calcium influx and mobilization from internal stores in stimulated human neutrophils. *J. Biol. Chem*. 1989; 264:1522–1527. [PubMed: 2536366]
- Murayama Y, Weber B, Saleem KS, Augath M, Logothetis NK. Tracing neural circuits in vivo with Mn-enhanced MRI. *Magn. Reson. Imaging*. 2006; 24:349–358. <http://dx.doi.org/10.1016/j.mri.2005.12.031>. [PubMed: 16677940]
- Narita K, Kawasaki F, Kita H. Mn and Mg influxes through Ca channels of motor nerve terminals are prevented by verapamil in frogs. *Brain Res*. 1990; 510:289–295. [PubMed: 2158851]
- Natt O, Watanabe T, Boretius S, Radulovic J, Frahm J, Michaelis T. High-resolution 3D MRI of mouse brain reveals small cerebral structures in vivo. *J. Neurosci. Methods*. 2002; 120:203–209. [PubMed: 12385770]
- Pautler RG. Biological applications of manganese-enhanced magnetic resonance imaging. *Methods Mol. Med*. 2006; 124:365–386. [PubMed: 16506430]
- Pautler RG, Koretsky AP. Tracing odor-induced activation in the olfactory bulbs of mice using manganese-enhanced magnetic resonance imaging. *NeuroImage*. 2002; 16:441–448. <http://dx.doi.org/10.1006/nimg.2002.1075>. [PubMed: 12030829]
- Pautler RG, Mongeau R, Jacobs RE. In vivo trans-synaptic tract tracing from the murine striatum and amygdala utilizing manganese enhanced MRI (MEMRI). *Magn. Reson. Med*. 2003; 50:33–39. <http://dx.doi.org/10.1002/mrm.10498>. [PubMed: 12815676]
- Pautler RG, Silva AC, Koretsky AP. In vivo neuronal tract tracing using manganese-enhanced magnetic resonance imaging. *Magn. Reson. Med*. 1998; 40:740–748. [PubMed: 9797158]
- Pelled G, Bergman H, Ben-Hur T, Goelman G. Manganese-enhanced MRI in a rat model of Parkinson's disease. *J. Magn. Reson. Imaging*. 2007; 26:863–870. <http://dx.doi.org/10.1002/jmri.21051>. [PubMed: 17896372]
- Paxinos, G., Watson, C. *The Rat Brain in Stereotaxic Coordinates Sixth Edition*. Academic Press; 2007.
- Roth TL, Nayak D, Atanasijevic T, Koretsky AP, Latour LL, McGavern DB. Transcranial amelioration of inflammation and cell death after brain injury. *Nature*. 2014; 505:223–228. <http://dx.doi.org/10.1038/nature12808>. [PubMed: 24317693]
- Saleem KS, Pauls JM, Augath M, Trinath T, Prause BA, Hashikawa T, Logothetis NK. Magnetic resonance imaging of neuronal connections in the macaque monkey. *Neuron*. 2002; 34:685–700. [PubMed: 12062017]
- Simmons JM, Saad ZS, Lizak MJ, Ortiz M, Koretsky AP, Richmond BJ. Mapping prefrontal circuits in vivo with manganese-enhanced magnetic resonance imaging in monkeys. *J. Neurosci*. 2008; 28:7637–7647. <http://dx.doi.org/10.1523/JNEUROSCI.1488-08.2008>. [PubMed: 18650340]
- Slout WN, Gramsbergen JB. Axonal transport of manganese and its relevance to selective neurotoxicity in the rat basal ganglia. *Brain Res*. 1994; 657:124–132. [PubMed: 7820609]
- Takeda A, Ishiwatari S, Okada S. In vivo stimulation-induced release of manganese in rat amygdala. *Brain Res*. 1998; 811:147–151. [PubMed: 9804933]
- Thuen M, Singstad TE, Pedersen TB, Haraldseth O, Berry M, Sandvig A, Brekken C. Manganese-enhanced MRI of the optic visual pathway and optic nerve injury in adult rats. *J. Magn. Reson. Imaging*. 2005; 22:492–500. <http://dx.doi.org/10.1002/jmri.20400>. [PubMed: 16161073]
- Van der Linden A, Van Meir V, Tindemans I, Verhoye M, Balthazart J. Applications of manganese-enhanced magnetic resonance imaging (MEMRI) to image brain plasticity in song birds. *NMR Biomed*. 2004; 17:602–612. <http://dx.doi.org/10.1002/nbm.936>. [PubMed: 15761949]

- Van der Linden A, Verhoye M, Van Meir V, Tindemans I, Eens M, Absil P, Balthazart J. In vivo manganese-enhanced magnetic resonance imaging reveals connections and functional properties of the songbird vocal control system. *Neuroscience*. 2002; 112:467–474. [PubMed: 12044464]
- Watanabe T, Michaelis T, Frahm J. Mapping of retinal projections in the living rat using high-resolution 3D gradient-echo MRI with Mn²⁺-induced contrast. *Magn. Reson. Med*. 2001; 46:424–429. [PubMed: 11550231]
- Watanabe T, Natt O, Boretius S, Frahm J, Michaelis T. In vivo 3D MRI staining of mouse brain after subcutaneous application of MnCl₂. *Magn. Reson. Med*. 2002; 48:852–859. <http://dx.doi.org/10.1002/mrm.10276>. [PubMed: 12418000]
- Watanabe T, Radulovic J, Spiess J, Natt O, Boretius S, Frahm J, Michaelis T. In vivo 3D MRI staining of the mouse hippocampal system using intracerebral injection of MnCl₂. *NeuroImage*. 2004; 22:860–867. <http://dx.doi.org/10.1016/j.neuroimage.2004.01.028>. [PubMed: 15193616]
- Yu X, Chung S, Chen DY, Wang S, Dodd SJ, Walters JR, Isaac JT, Koretsky AP. Thalamocortical inputs show post-critical-period plasticity. *Neuron*. 2012; 74:731–742. <http://dx.doi.org/10.1016/j.neuron.2012.04.024>. [PubMed: 22632730]
- Yu X, Koretsky AP. Interhemispheric plasticity protects the deafferented somatosensory cortex from functional takeover after nerve injury. *Brain Connect*. 2014; 4:709–717. <http://dx.doi.org/10.1089/brain.2014.0259>. [PubMed: 25117691]
- Yu X, Zou J, Babb JS, Johnson G, Sanes DH, Turnbull DH. Statistical mapping of sound-evoked activity in the mouse auditory midbrain using Mn-enhanced MRI. *NeuroImage*. 2008; 39:223–230. <http://dx.doi.org/10.1016/j.neuroimage.2007.08.029>. [PubMed: 17919926]

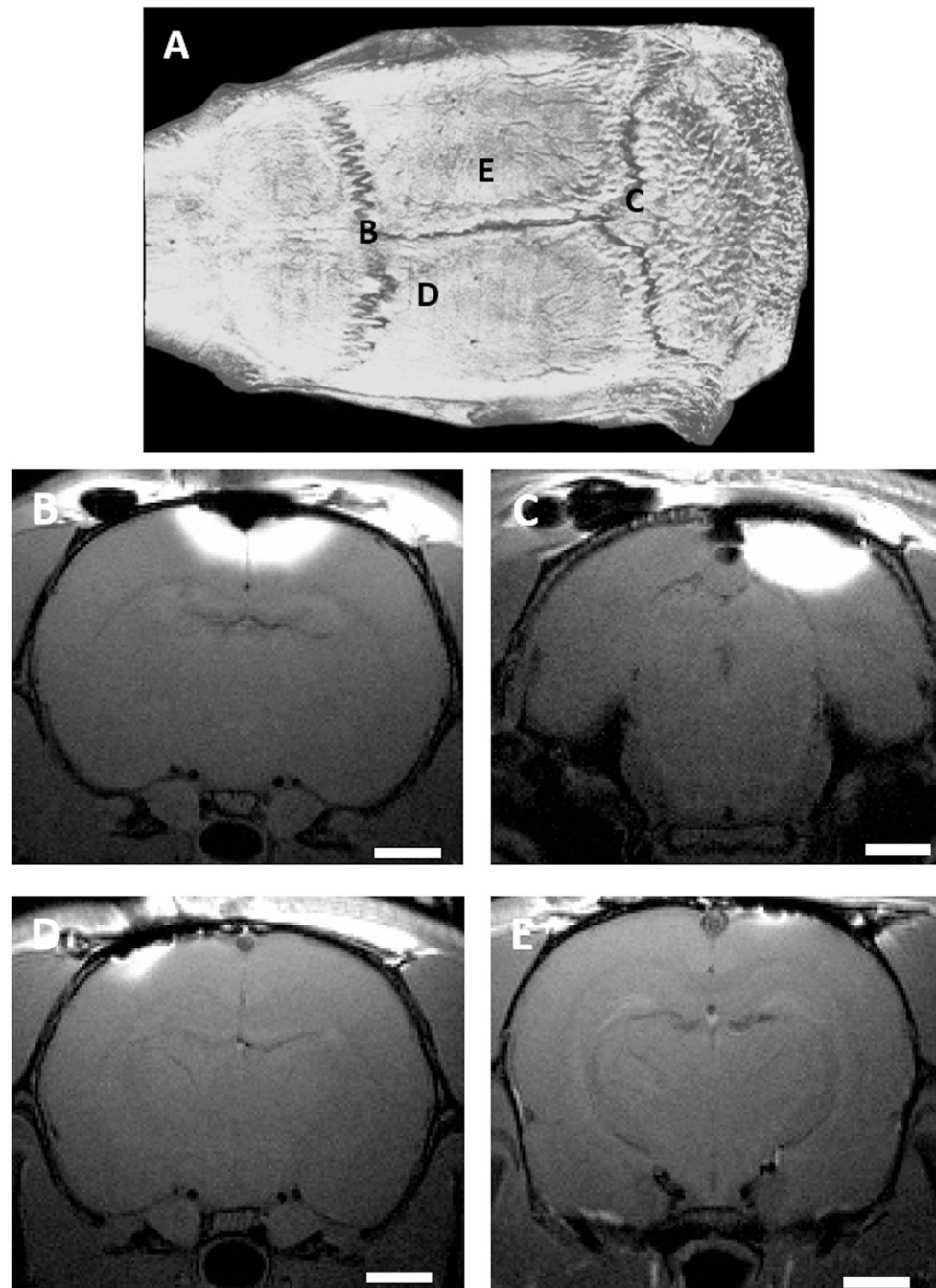


Fig. 1. Location dependence of transcranial manganese delivery efficiency
 CT image of a rat skull (A) and T₁ - weighted MR images of rats receiving 500 mM solution of MnCl₂ on the bregma (B), on the lambda (C), left side close to S1 (D), approximately -1.4 mm posterior from bregma and lateral -2 mm, and right side away from the bregma (E), approximately -5 mm posterior from bregma and lateral +3 mm. Scale bar, 2 mm. Images are representative of three rats per group.

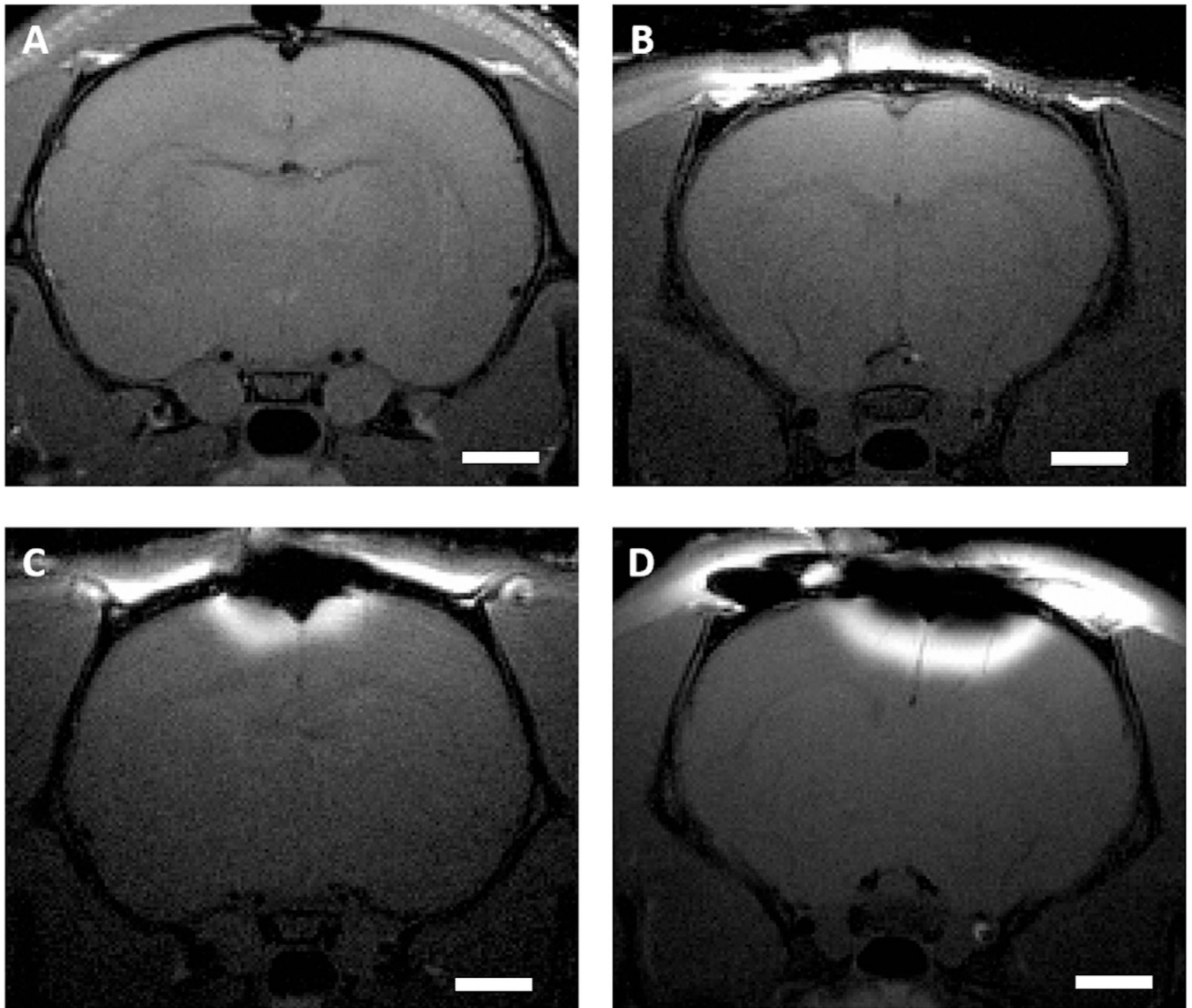


Fig. 2. Concentration dependence of transcranial manganese delivery efficiency
T₁ - weighted MR images of rats receiving - (A) control solution (slice shown is approximately -2.5 mm posterior from bregma), (B) 100 mM MnCl₂ (slice shown is approximately 1.5 mm anterior from bregma), (C) 250 mM MnCl₂ (slice shown is approximately -0.5 mm posterior from bregma), and (D) 500 mM MnCl₂ (slice shown is approximately -0.5 mm posterior from bregma) on the bregma. Scale bar, 2 mm. Images are representative of three rats per group.

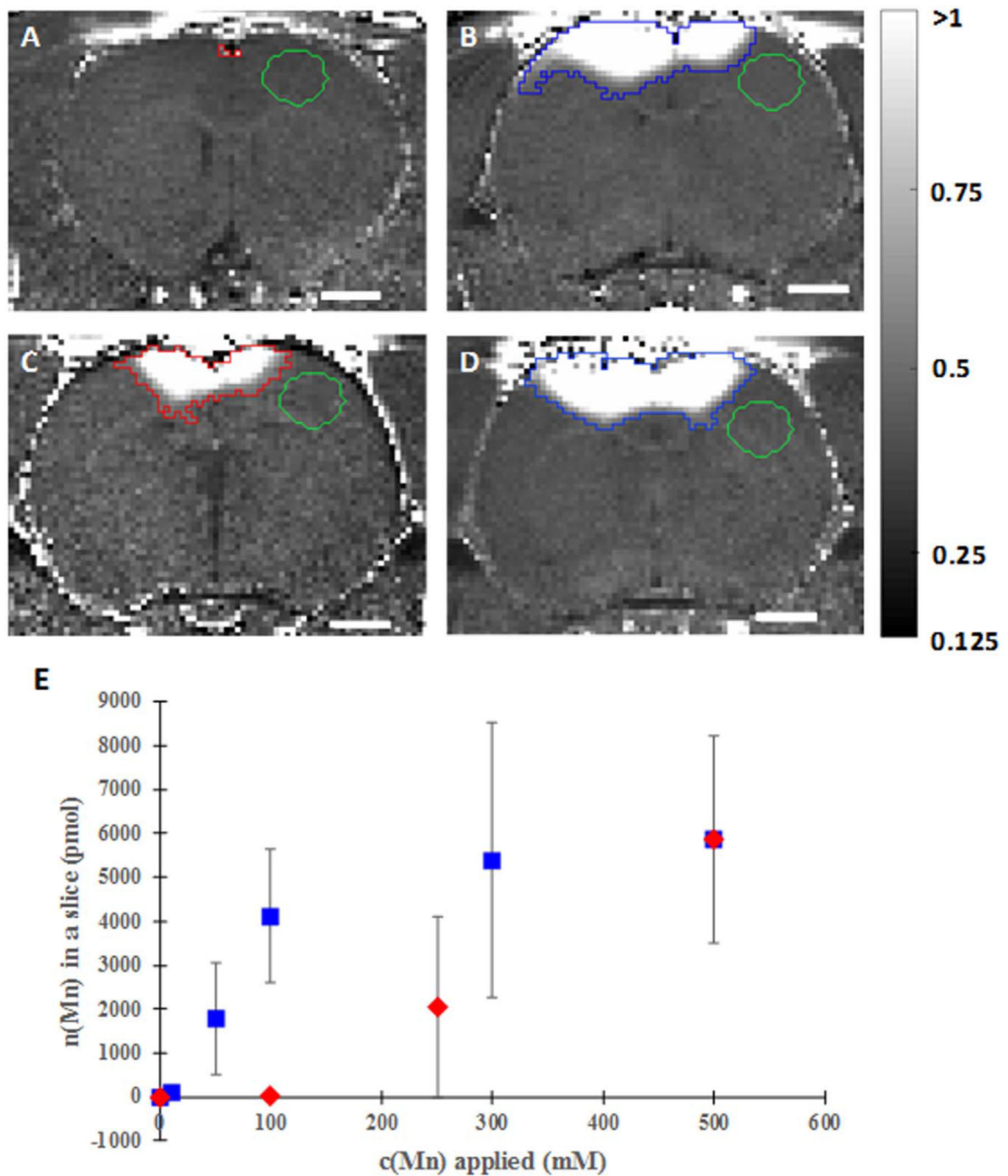


Fig. 3. Concentration dependence and the calcium addition effect on transcranial manganese delivery efficiency

R₁-maps calculated from saturation recovery MR images of rats receiving - (A) 100 mM MnCl₂ (slice shown is approximately 1.5 mm anterior from bregma), (B) 100 mM MnCl₂+400 mM CaCl₂ (slice is approximately -0.6 mm posterior from bregma), (C) 250 mM MnCl₂ (slice shown is approximately -0.5 mm posterior from bregma) and (D) 300 mM MnCl₂+200 mM CaCl₂ (slice shown is approximately -0.6 mm posterior from bregma) on the bregma and dependence of total amount of manganese delivered to the brain on the concentration of manganese solution applied on the bregma, when only MnCl₂ was applied

(red diamonds) and when CaCl_2 was added to the total concentration of 500 mM (blue squares) (E). Scale bar, 2 mm. R_1 intensity scaling, $0.125\text{--}1\text{ s}^{-1}$. ROIs where T_1 measurements were made are shown on the top of the R_1 maps in red or blue, whereas the green ROIs represent the background. Ca^{2+} increases the efficiency of Mn^{2+} delivery through the skull. Each data point represents the average of three animals.

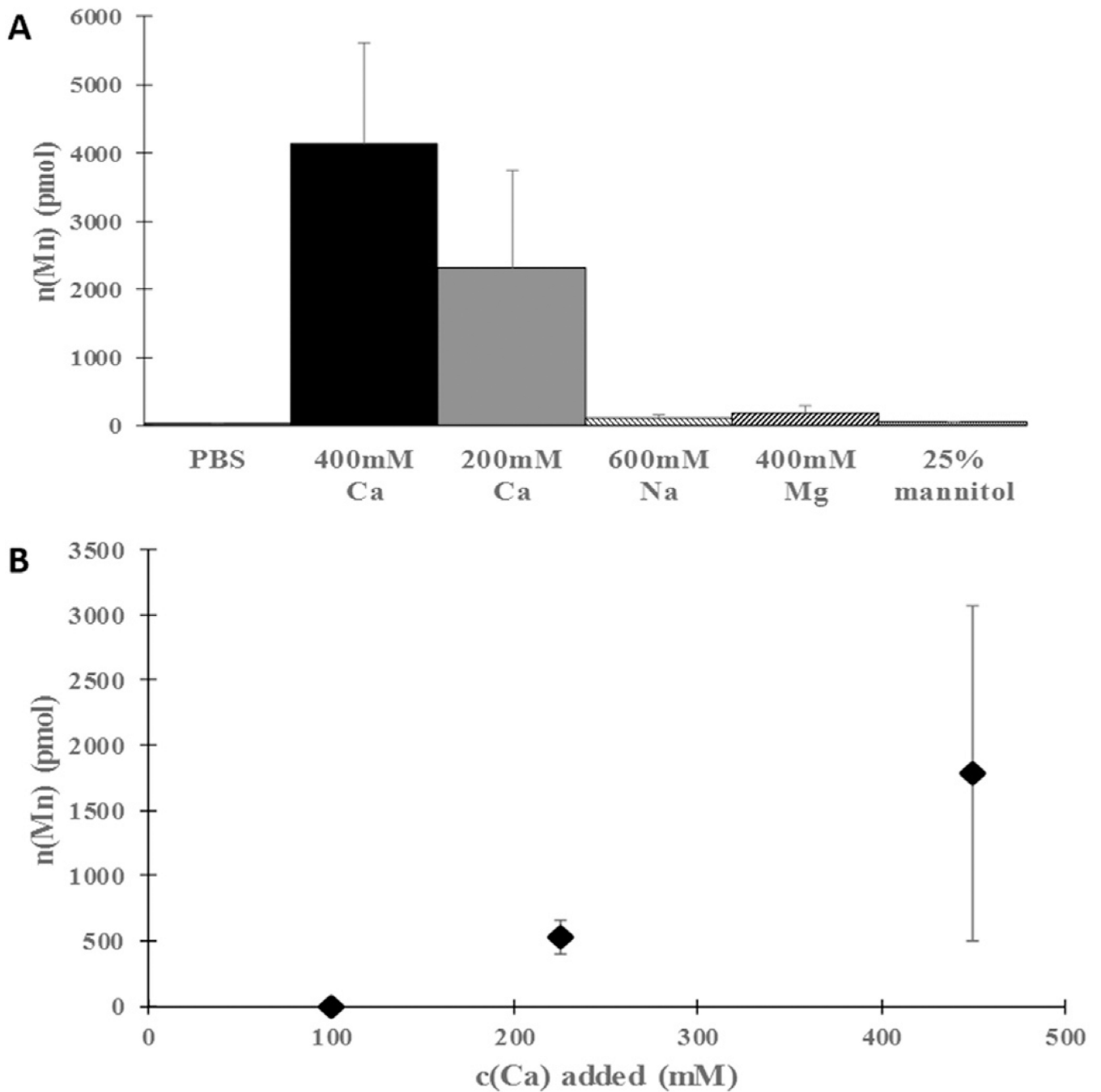


Fig. 4. Influence of type and concentration of substances added to a manganese solution on transcranial manganese delivery efficiency

(A) Dependence of the total amount of manganese delivered to the brain when 100 mM MnCl_2 was applied on the bregma on the type and concentration of various compounds added to the manganese solution. Ca^{2+} significantly increased the efficiency, whereas Na^+ , Mg^{2+} and mannitol had a small effect on the efficiency of Mn^{2+} delivery. (B) Dependence of total amount of manganese delivered to the brain when 50 mM MnCl_2 was applied on the bregma on the amount of calcium salt added to the manganese solution. As the calcium

amount was lowered so was the efficiency of transcranial Mn^{2+} delivery. Each data point represents the average of three animals.

Author Manuscript

Author Manuscript

Author Manuscript

Author Manuscript

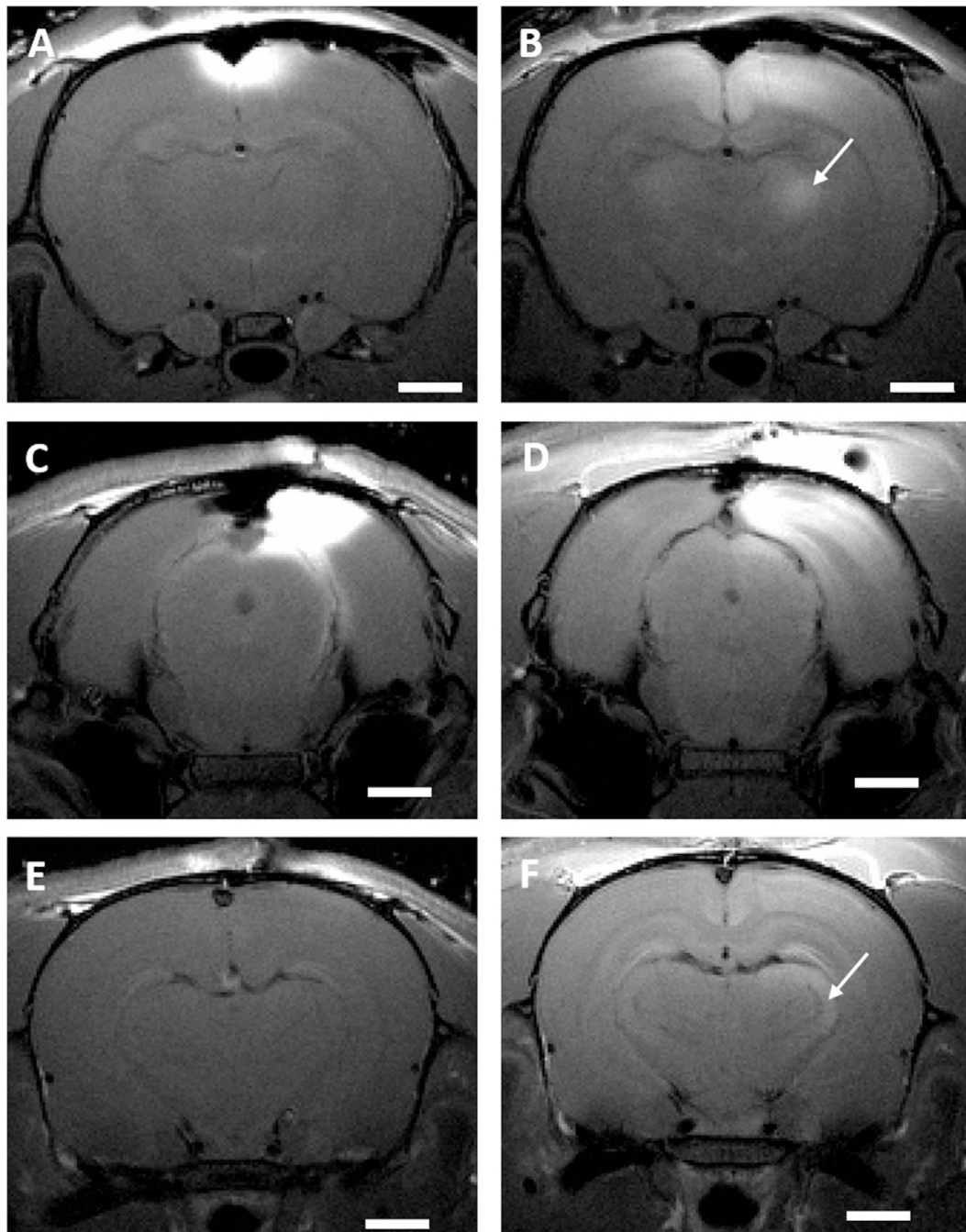


Fig. 5. Neuronal tract tracing with transcranially delivered manganese

T₁ - weighted MR images of rats receiving: 500 mM solution of MnCl₂ on the bregma immediately after solution application (A), as well as of 24 h after administration (B), solution of 250 mM MnCl₂ and 250 mM CaCl₂ on the lambda immediately after solution application (C), (E) ((C) and (E) represent two different slices) as well as of 24 h after administration (D), (F). Scale bar, 2 mm. The white arrows indicate the location of thalamic nuclei to which manganese has traced 24 h after application. Images are representative of three rats per group.

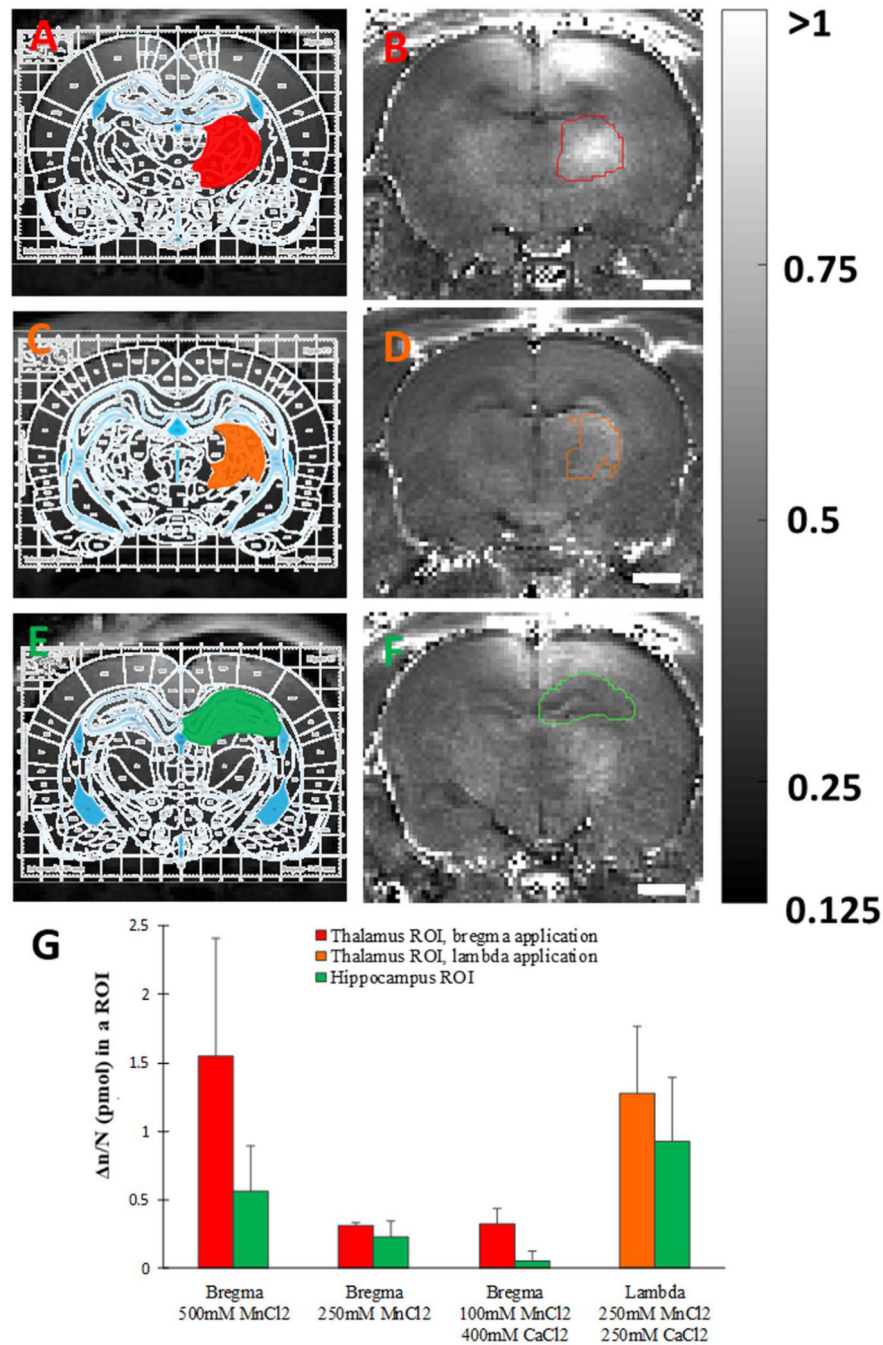


Fig. 6. Quantification of tract tracing with transcranially delivered manganese ROI determination by overlaying of registered rat brain atlas (Paxinos and Watson (2007), 6th edition) with saturation recovery MR images of rats obtained 24 h after receiving 500 mM solution of MnCl₂ on the bregma (A,E) or 250 mM MnCl₂ and 250 mM CaCl₂ on the lambda (C) and subsequent ROI overlay on corresponding R₁ maps calculated from those images (B,D,F); and calculated difference per voxel of manganese amounts ($\Delta n/N$) in the thalamus and hippocampus ROIs between 24 h after manganese application and immediately after the application (G). Red and orange colors correspond to thalamus ROIs for bregma

and lambda manganese application, respectively, while green color corresponds to hippocampus ROIs in both cases. Scale bar, 2 mm. R_1 intensity scaling, $0.125-1 \text{ s}^{-1}$. Each data point represents the average of three animals.